Sebastian Walde (Autor)

AlN base layers for UV LEDs

66

Innovationen mit Mikrowellen & Licht

Forschungsberichte aus dem

Ferdinand-Braun-Institut,
Leibniz-Institut
für Höchstfrequenztechnik

AlN base layers for UV LEDs

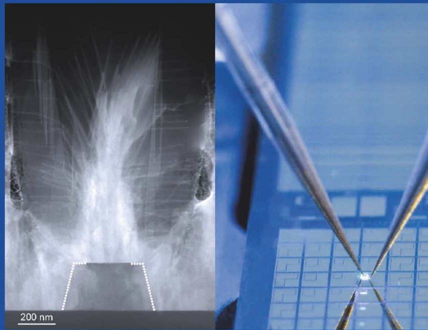

Sebastian Walde

https://cuvillier.de/de/shop/publications/8472

Copyright:
Cuvillier Verlag, Inhaberin Annette Jentzsch-Cuvillier, Nonnenstieg 8, 37075 Göttingen, Germany
Telefon: +49 (0)551 54724-0, E-Mail: info@cuvillier.de, Website: https://cuvillier.de

CHAPTER 1

Fundamentals

In this chapter the basic physical background will be given for the preparation of the AlN base layers including the crystal structure of AlN and the heteroepitaxial relation between AlN and sapphire. Further, the impact of specific properties of the AlN base layers on the performance of UV LED heterostructures grown on top will be discussed with the aim to define certain quality criteria for the AlN base layers regarding the suitability of being used as UV LED templates. Additionally, the state of research in the field of AlN base layers will be outlined to put this work in the context of related literature.

1.1 Heteroepitaxial growth of AlN on sapphire

Prior to describing the heteroepitaxial growth of AlN on sapphire, an answer to the intuitive question will be given why AlN is grown heteroepitaxially on sapphire and why not native AlN bulk substrates are used as base layers similar to other III-V semiconductor material systems, e.g. based on GaAs [28]. Also for the III-nitride material GaN the usage of GaN bulk substrates becomes increasingly popular [29]. However, in case of AlN still many challenges in the complex process of growing AlN bulk substrates have to be overcome. AlN bulk substrates are usually grown by physical vapour transport at temperatures above 2000 °C [30]. In the past a lot of progress has been made in the preparation of AlN bulk substrates in terms of wafer size and crystal quality [31, 32]. However, one of the main issue is still the lack of transparency in the relevant UV range which is ascribed to impurities built in during growth [33–35]. The heteroepitaxial growth of AlN on sapphire instead is a straightforward technology to

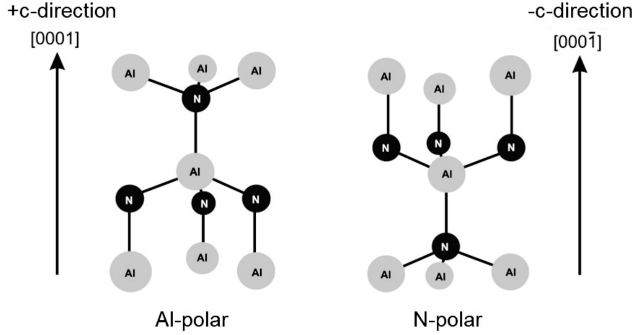

Figure 1.1: Schematic structure of wurtzite AlN in $+c$ and $-c$ direction resulting in Al- and N-polarity, respectively. From reference [42] with permission of Cuvillier © 2014.

go for, since it is similar to the heteroepitaxial growth of GaN on sapphire which is well established in the industrial manufacturing process of GaN-based blue LEDs [36]. Despite the lattice mismatch, GaN and also AlN grow reasonably well on sapphire while sapphire substrates themselves are available in large sizes at low cost [37].

AlN usually has the hexagonal wurtzite crystal structure shown in Fig. 1.1 with lattice constants $a_{\mathrm{AlN}} = 0.3111\,\mathrm{nm}$ and $c_{\mathrm{AlN}} = 0.4981\,\mathrm{nm}$ [38]. The band gap of AlN is relatively high with 6.1 eV [39]. In Fig. 1.1 it can be seen that the $+c$ and $-c$ directions lead to a different arrangement of the Al and N atoms to each other determining the polarity [40]. By definition, in Fig. 1.1 the $+c$ direction is Al-polar, while the $-c$ arrangement is N-polar. Since AlN of Al-polarity or N-polarity show different properties, it is crucial to control the polarity [41]. In this work the desired phase is Al-polarity. The sapphire substrates (α-Al_2O_3) have a trigonal corundum crystal structure with lattice constants $a_{\mathrm{Al_2O_3}} = 0.4758\,\mathrm{nm}$ and $c_{\mathrm{Al_2O_3}} = 1.298\,\mathrm{nm}$ [43]. In this work AlN is grown on (0001) sapphire. Similar to GaN on (0001) sapphire, AlN will grow on the (0001) sapphire surface with (0001) orientation but with a unit cell rotated around the [0001] axis by an angle of 30° in relation to the underlying sapphire to compensate for the different atomic arrangement [44–47]. The atomic arrangement of the rotated unit cells can be seen in Fig. 1.2a. The Al-Al distance of the AlN in [100] direction will adapt to the Al-Al distance of the sapphire in [1$\bar{1}$0] direction. This results in an effective in-plane lattice constant of the sapphire of $a_{\mathrm{Al_2O_3}}/\sqrt{3}$ to which the AlN with

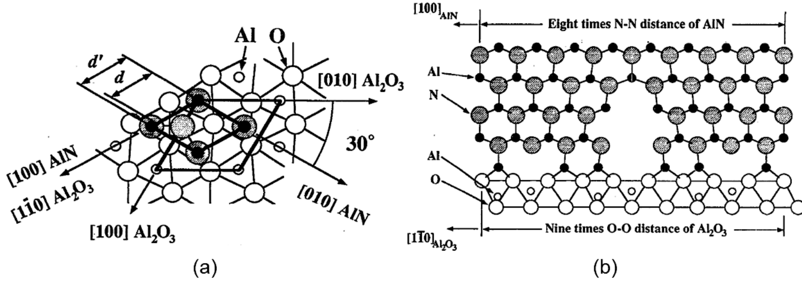

Figure 1.2: Illustration of the heteroepitaxial relation between AlN and sapphire in **(a)** plan view and **(b)** cross section. The AlN nucleates with a unit cell rotated by an angle of 30° with respect to the unit cell of the underlying sapphire. The resulting lattice mismatch of 13.29 % leads to 9 times the Al-Al distance of Al_2O_3 fitting to eight times the Al-Al distance of AlN combined with an edge dislocation in the center. From reference [48] with permission of AIP Publishing © 1994.

lattice constant a_{AlN} needs to adapt. This yields a lattice mismatch f of

$$f = \frac{a_{\mathrm{AlN}} - a_{\mathrm{Al_2O_3}}/\sqrt{3}}{a_{\mathrm{Al_2O_3}}/\sqrt{3}} = 13.29\,\%. \tag{1.1}$$

The lattice mismatch leads to growth according to nine times the Al-Al distance of Al_2O_3 fitting to eight times the Al-Al distance of AlN combined with an edge dislocation in the center depicted in Fig. 1.2b. This reduces the effective lattice mismatch after several monolayers.

Due to the large lattice mismatch AlN almost immediately grows in 3-dimensional growth mode on top of the sapphire leading to independent nucleation islands instead of a continuous 2-dimensional layer [49–51]. A 2-dimensional layer is formed only after subsequent AlN growth until coalescence of the nucleation grains is reached. The independent 3-dimensional nucleation grains lead to a certain distribution of tilt and twist between them. At the point of their coalescence, tilt and twist result in low angle grain boundaries which are compensated by the generation of a huge amount of threading dislocations (TDs) with a density above $1 \times 10^{10}\,\mathrm{cm}^{-2}$ [52–55]. Dislocations are one-dimensional line defects which are characterised by their Burgers vector $\vec{b}$ and line vector $\vec{l}$. The line vector l points along the core of the dislocation which is the center of the imperfection of the lattice. A TD names a dislocation for which the line vector has a component in growth direction so that the dislocation penetrates through the layer in growth direction. The Burgers vector can be determined by drawing a closed

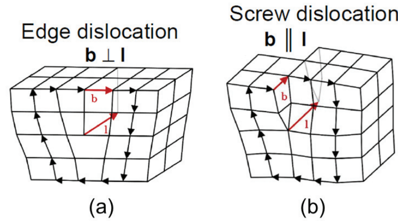

Figure 1.3: Sketch of **(a)** an edge dislocation and **(b)** a screw dislocation. An edge dislocation is associated with an extra half plane inside the crystal lattice, while a screw type dislocation is associated with a distortion of crystal planes to each other. From reference [56] with permission of Springer Nature © 2013.

path in the perfect lattice of a crystal and then again in the disturbed lattices with the closed path encircling the dislocation. The same path which was closed in the perfect lattice will be open in the lattice with the dislocation. The difference between the two closed paths is the Burgers vector. This method to determine the Burgers vector is visualised in Fig. 1.3 for the two basic kinds of dislocations, the edge dislocation and the screw dislocation. The edge dislocation is associated with an extra half plane inserted in the crystal lattice. The definition of an edge type dislocation is that the Burgers vector $\vec{b}$ is perpendicular to the line vector $\vec{l}$. The screw dislocation is associated with a distortion of the crystal planes to each other. The definition of a screw dislocation is that the Burgers vector $\vec{b}$ is parallel to the line vector $\vec{l}$. Geometrically, edge dislocations compensate twist of the nucleation grains, while screw dislocations compensate tilt. A dislocation for which the Burgers vector $\vec{b}$ is neither perpendicular nor parallel to the line vector $\vec{l}$ is called mixed dislocation.

If dislocations meet, they will react with each other under the condition that the overall Burgers vector is conserved [57]. This translates to the equation

$$\sum_i \vec{b}_i = \sum_j \vec{b}_j \,, \tag{1.2}$$

with $\vec{b}_i$ being the Burger vectors of the incoming dislocations and $\vec{b}_j$ being the Burgers vectors of the outgoing dislocations. For two dislocations with opposite Burgers vectors the sum over the Burgers vectors is zero. This process is called annihilation and results in an overall dislocation reduction.

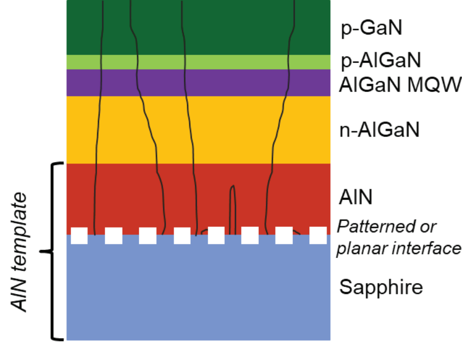

Figure 1.4: Simplified layer stack of a UV LED heterostructure including the AlN template with planar or patterned AlN/sapphire interface. The active region with the MQW lies between the n-side and p-side of the device. TDs (dislocations penetrating through the heterostructure) are indicated by the black lines. The light is usually extracted via the sapphire substrate due to the absorbing p-GaN.

1.2 AlN templates as UV LED base layers

The AlN templates consist of (0001) AlN grown on (0001) sapphire, also called *c*-plane AlN and *c*-plane sapphire. They are used as the foundation for subsequently deposited UV LED heterostructures. Usually, the AlN template is grown in a first epitaxial growth run separated from the second growth run to grow the UV LED heterostructure on top. In Fig. 1.4a the simplified layer stack of a typical UV LED heterostructure including the underlying AlN template is shown. In general, an LED heterostructure consists of the pn-junction and the quantum wells between the p- and n-side forming the active region of the LED [58–61]. In case of the UV LED heterostructure on top of the AlN template, the n-side is grown with silicon-doped AlGaN. The following active region is formed by the multi-quantum-well (MQW) stack whereas each quantum well is separated by the barriers. The p-side on top of the MQW stack starts with a magnesium-doped p-AlGaN capped by a magnesium-doped p-GaN layer. The light is generated by electrical contacting so that electrons and holes are injected via the n-side and p-side, respectively. Accumulation of electrons and holes in the MQW leads to increasing probability of radiative recombination in the MQW. This results in photon emission with the characteristic wavelength of the quantum wells. The crucial question is now, how the properties of the AlN template will influence the performance of the UV LED heterostructure. Before this can be evaluated the performance of an LED needs to be defined. The ratio between the input carrier pairs and the extracted photons is

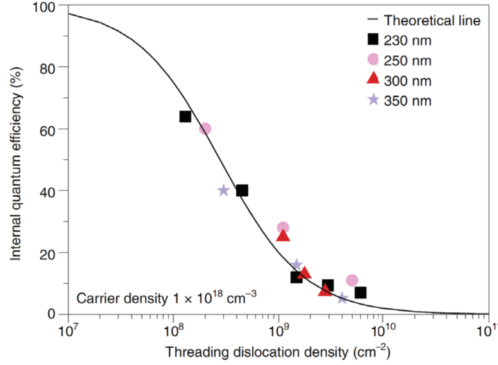

Figure 1.5: Simulated data combined with experimental results for the dependency between internal quantum efficiency and the TDD for a constant carrier density of $1 \times 10^{18}\,\mathrm{cm}^{-3}$. The experimental results are in good agreement with the cure predicted by the simulation. From reference [62] with permission of Springer Nature © 2019.

the external quantum efficiency η_{EQE} which fulfils the following relation

$$\eta_{\mathrm{EQE}} = \eta_{\mathrm{rad}} \cdot \eta_{\mathrm{inj}} \cdot \eta_{\mathrm{LEE}} = \eta_{\mathrm{IQE}} \cdot \eta_{\mathrm{LEE}}. \tag{1.3}$$

The radiative efficiency η_{rad} is the ratio between the radiative recombination inside the MQW and other for instance non-radiative recombination processes. The injection efficiency η_{inj} describes how efficient the injected electrons and holes reach the MQW and accumulate inside. The product of η_{rad} and η_{inj} is the internal quantum efficiency η_{IQE}. The ratio of the generated photons, which are extracted out of the LED heterostructure, in relation to all generated photons inside the MQW is the light extraction efficiency η_{LEE}. The AlN base layer has a great influence on all of these parameters. The focus of this work lies on the influence of the radiative efficiency η_{rad} and the light extraction efficiency η_{LEE}. The impact of the properties of the AlN templates on these parameters will be briefly discussed in the following.

Crystal quality As mentioned before, the crystal quality of the AlN base layers is mainly defined by the amount of TDs. TDs will penetrate through the whole layer stack as indicated in Fig. 1.4. Inside the MQW they will lead to non-radiative recombination which directly limits the radiative efficiency η_{rad}. In Fig. 1.5 the effect of the threading dislocation density (TDD) on the radiative efficiency is quantified assuming a constant carrier density of $1 \times 10^{18}\,\mathrm{cm}^{-3}$. Theoretical calculations of the internal quantum

efficiency in dependency of the TDD in the active region are presented and compared with experimental results for UV LEDs of different wavelengths [63–69]. If the TDD is reduced from $1 \times 10^{10}\,\mathrm{cm}^{-2}$ down to $1 \times 10^{8}\,\mathrm{cm}^{-2}$ the IQE is predicted to increase from approx. 2 % to approx. 75 %. The reduction of the TDD can be considered as one of the most important tasks for achieving high performance LEDs. For pseudomorphic growth of the UV LED heterostructure on the AlN template at least up to the active region, the TDD in the active region is determined by the TDD of the underlying AlN template. The TDD will also have an influence on the injection efficiency η_{inj}. Usually, layers with lower TDD show better conductivity [70].

Surface morphology In terms of surface morphology it is important to provide a continuous and homogeneous surface, since usually any disturbance of the AlN surface will be directly translated to the subsequently grown AlGaN. Additionally, the layer should be reasonably smooth to suppress inhomogeneous AlGaN growth of different compositions. Inhomogeneous AlGaN growth results in broadening of the emission peak of the related UV LED. Furthermore, a rough AlN surface leads to rough AlGaN growth inducing smearing out of the MQW which decreases carrier localisation and thus, radiative recombination. Usually, the optimal condition for the AlN surface morphology is an atomically smooth surface, since this is a good basis for reproducible heterostructure growth. However, there also has been work of providing AlN base layers with a heavily step bunched surface. Inhomogeneous AlGaN incorporation leads to a broad peak with an increased integrated emission power [71]. However, in this work a narrow peakwidth of the final UV LEDs is desired.

AlN/sapphire interface Up to now, a p-doped GaN layer is normally used for electrical contacting at the p-side. This layer is absorbing in the UV range due to the bandgap of GaN being 3.4 eV which translates to a band edge of approx. 360 nm [72]. Hence, 50 % of the generated light will be lost in the p-side. The other 50 % of the generated light will propagate towards the transparent AlN template where part of it will be extracted. However, the refractive index profile of AlN and sapphire results in total reflection so that a huge portion of the light is reflected back into the structure and absorbed in the p-side. To soften this total reflection the shape of the AlN/sapphire interface plays an important role. By implementing a patterned AlN/interface, increased scattering has the potential of improving the light extraction efficiency. A patterned interface can be achieved by epitaxial lateral overgrowth. This also enables efficient defect reduction. However, the criterium of a smooth AlN surface is challenging to achieve, since the

layer needs to properly coalesce.

Strain state The growth of the UV LED heterostructure on top of an AlN template is always accompanied by the formation of strain, since AlGaN has a larger in-plane lattice constant compared to AlN. If during growth the strain becomes too high, the layer will relax by for instance roughening or the formation of new TDs which becomes energetically favourable. For growth of UVA and UVB heterostructures, the Ga-content needed is too high for pseudomorphic. Thus, relaxation will be achieved in a controlled way by appropriate strain management to generate as few new TDs as possible. In contrast, UVC LED heterostructures consist of AlGaN with high Al-content so that the heterostructure usually can be grown pseudomorphically up to the active region without any relaxation. However, the process always works on the edge of relaxation, since only a small increase in Ga-content in the n-AlGaN layer leads to a considerable improvement of the electrical conductivity. Hence, it is obvious that the strain state of the AlN buffer always has to be considered in order to be able to appropriately handle the strain during subsequent AlGaN growth. For AlN base layers with different strain states resulting in slightly different lattice constants at growth temperature, the desired layer is the one with the biggest in-plane lattice constant, since AlGaN has a bigger lattice constant than AlN.

These four criteria will be discussed along the scientific results of this work. While in literature the main focus often only lies on the reduction of the TDD, in this work the other criteria will also be considered.

1.3 State of research

In this section the state of research regarding preparation of AlN base layers for UV LEDs will be outlined [73]. After giving a short overview of the general field of planar AlN growth, the focus lies on the specific research topics of HTA and growth on patterned substrates. These methods have gained increasing research interest in recent years and are also the main focus of this work. The relevant literature of these methods will be sorted in work that was published before the start of this work in June 2017 and after. What has to be noted is that it is often difficult to compare different research work, since methods for instance for the determination of the TDD strongly differ. While determination by for instance transmission electron microscopy has to be carefully

examined regarding the thickness of the specimen and the incident angle of the electron beam, the measurement of the X-ray omega rocking curve full width at half maximum (XRC-FWHM) by X-ray diffraction (XRD) is a more reliable method to get a benchmark of the related TDD.

Planar AlN growth Planar AlN growth is here referred to as AlN growth on planar sapphire without any post-thgrowth annealing step, since this will be described later in more detail. AlN growth on sapphire has a long history with work dating back to before the year 2000 [74]. Besides MOVPE growth there has been work also using hydride vapour phase epitaxy [75, 76] and molecular beam epitaxy [77]. Using MOVPE the polarity control at growth start during nucleation is crucial for the quality of the subsequently grown AlN. The ratio of Al-polar to N-polar AlN is influenced by the amount of oxygen in the reactor atmosphere [78–81]. Also the preflow (trimethylaluminium or nitridation) prior to the growth plays an important role [82, 83]. After successful nucleation the main mechanism for TDD reduction is increasing the layer thickness to induce mutual annihilation of TDs. Unfortunately, the AlN on sapphire layer system usually exhibits a high amount of tensile strain during growth which leads to layer cracking at thin layer thickness if no strain management is applied [84]. The strain management is usually done by inducing alternating 2D to 3D growth transitions in the AlN layer resulting in alternating roughening and smoothing of the layer. This can be done by different techniques which by changing the growth conditions will create a multilayer system for instance by the ammonia pulse-flow method or by varying the V/III ratio etc. [66, 84–87]. AlN layer thickness of up to 4 µm and resulting TDDs in the range of mid $10^8\,\mathrm{cm}^{-2}$ can be reached by these methods.

Growth on patterned substrates The first reports about AlN growth on patterned sapphire substrates date back to 2006 [88, 89]. A trench pattern in the micrometre range was used and the TDD determined by plan-view TEM is presented to be below $10^7\,\mathrm{cm}^{-2}$ [89]. However, the related XRC-FWHM of 300″ for the 0002 reflection and 400″ for the 20-24 reflection suggest a TDD in the range of approx. $1 \times 10^9\,\mathrm{cm}^{-2}$ range. In the late 2000s and early 2010s the AlN growth on stripes was established by different groups with similar results [90, 91]. In recent years it was shown that in case of GaN it can be very beneficial to go for patterned sapphire substrates with patterns in the nanometre range (NPSS) [92, 93]. First demonstrations of overgrowing NPSS by AlN were presented by Dong et al. in 2013 [94, 95]. They used nanosphere lithography to prepare the hole type nanopattern on the sapphire surface and ended up with a TDD of

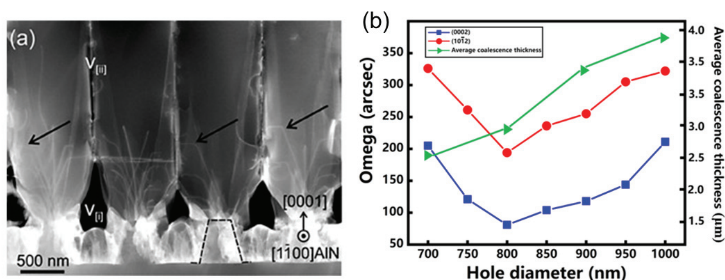

Figure 1.6: (a) TEM micrograph showing the growth start of AlN on nanopillar patterned sapphire with pattern pitch of 1 µm. From reference [97] with permission of John Wiley and Sons © 2016. **(b)** XRC-FWHM of the 0002 and 10-12 reflections and the average coalescence thickness against the hole diameter for AlN growth on nanohole patterned sapphire substrates with a constant pitch of 1.4 µm. From reference [100] with permission of The Japan Society of Applied Physics © 2019.

the subsequently grown AlN of $1.2 \times 10^9\,\text{cm}^{-2}$ estimated by calculation from the XRC-FWHM of 86″ for the 0002 reflection and 320″ for the 10-12 reflection. Subsequently grown UV LED heterostructures emitting at 282 nm showed an increase in the external quantum efficiency of 98 % compared to a flat sapphire substrate. More work from different groups followed with growth on nanoholes as well as nanopillars [96–99]. The lowest TDD achieved was as low as approx. $3.5 \times 10^8\,\text{cm}^{-2}$ determined by selective defect etching. This is in agreement with the XRC-FWHM of 171″ for the 0002 reflection and 205″ for the 10-12 reflection. The main reduction mechanisms are the bending of TDs to the free surfaces at growth start as well as the approximately defect free growth in the laterally overgrown regions as can be seen in the TEM image in Fig. 1.6a.

After June 2017 further work focused on further TDD reduction by finding the optimal pattern dimensions for reducing the area of coalescence in relation to the laterally overgrown regions, since coalescence fronts can lead to new TDs [100, 101]. In Fig. 1.6b the XRC-FWHM of the 0002 and 10-12 reflections and the average coalescence thickness are plotted against the hole diameter for a constant pattern pitch of 1.4 µm. For a hole diameter of 800 nm, XRC-FWHM of 162″ for the 0002 reflection and 181″ for the 10-12 reflection were measured which translates to a TDD of approx. $2.8 \times 10^8\,\text{cm}^{-2}$.

HTA of AlN/sapphire HTA of AlN/sapphire emerged in 2016. The group of Prof. Miyake at the Mie university in Japan published first results about this method in early 2016 [102–104]. They annealed a 300 nm thick AlN MOVPE layer on sapphire in a carbon-saturated N_2-CO atmosphere at 1700 °C for 1 h and observed a reduction